EUROPEAN ORGANIZATION FOR NUCLEAR RESEARCH

CERN PPE/92-131
July 30, 1992

Isolated Hard Photon Emission in Hadronic Z^0 Decays

L3 Collaboration

Abstract

We report on a study of energetic, isolated photons in a sample of $\sim$ 320k Z^0 hadronic decays. Energetic isolated photons probe the short distance structure of QCD. We compare our data with the prediction of several QCD-based calculations.

A search for new processes with one or two photons in the hadronic final state is also presented. No evidence for physics beyond the standard model is found.

(submitted to Phys. Lett.)

1 Introduction

The study of energetic, isolated photons (direct photons) in hadronic Z^0 decays at LEP offers an important probe of the short-distance structure of QCD [1]. Although the elementary processes of photon and gluon emission are closely related, photons have the advantage of appearing directly in the final state, whereas gluons undergo a complex evolution into hadrons. In addition to their value as probes of perturbative QCD and QED, direct photons serve as signatures of new physical phenomena.

Previous studies of final state radiation at lower energy e^+e^- colliders [2] were limited by a large contamination due to photons radiated from the initial state electrons and positrons. At the Z^0 resonance this background is strongly suppressed, making LEP an ideal laboratory for this study. The primary background to direct photons at LEP is the decay of energetic neutral hadrons into photons which are unresolved in the detector.

We report here on the results of an analysis of energetic and isolated photons in hadronic events collected at LEP with the L3 detector during the 1990 and 1991 runs.

We present comparisons with theoretical models. Two complementary approaches are currently available for a theoretical description of final state quark radiation produced at the Z^0 resonance: matrix element and leading logarithm (or parton shower) methods. In the matrix element approach, the cross section is expanded systematically in powers of the electromagnetic coupling constant, α, and the running strong coupling constant, α_s [3]. In the leading logarithm approach, the cross section is expanded to all orders in the coupling constants, but only the leading logarithmic terms are used. These logarithmic terms dominate the cross section for collinear and soft radiation, and this is the limit in which this approach is strictly applicable. A smooth extrapolation to hard and isolated radiation is possible, but not necessarily accurate. Several Monte-Carlo programs are available for describing the leading logarithmic structure of the cross section with an iterative branching scheme; we present results using the programs: ARIADNE [4], HERWIG [5] and JETSET [6]. These programs differ in the variables they use for a leading logarithmic expansion of the cross section, but all perform an ad-hoc matching of the first branch to the appropriate first order matrix element ($\mathcal{O}(\alpha)$ for a $q \to q\gamma$ branch, $\mathcal{O}(\alpha_s)$ for a $q \to qg$ branch). The modelling of the hadronization effects is the same in ARIADNE and JETSET, but different in HERWIG.

We have also determined limits for three new processes involving one or two hard photons in the final state:

- $Z^0 \to Y\gamma$ where Y is a narrow resonance decaying into hadrons.
- Excited quark production.
- $Z^0 \to Sq\bar{q}$ with $S \to \gamma\gamma$ where S is a scalar boson.

2 The L3 Detector

The L3 detector [7] consists of a central tracking chamber (TEC), a high resolution electromagnetic calorimeter composed of bismuth germanium oxide crystals, a ring of scintillation counters, a uranium and brass hadron calorimeter with proportional wire chamber readout, and an accurate muon chamber system. These detectors are installed in a 12 m diameter, 16 m long magnet, which provides a uniform field of 0.5 T along the beam direction.

The material in front of the electromagnetic calorimeter amounts to less than 10% of a radiation length. The energy resolution for electrons and photons is better than 2% for energies above 1.5 GeV. The angular resolution for electromagnetic clusters with energy above 5 GeV is better than 2 mrad.

3 Selection of Hadronic Events with Hard Photons

The primary trigger for hadronic events requires a total energy of 15 GeV in the calorimeters. This trigger is in logical OR with another trigger using only the barrel scintillation counters and also with a charged-track trigger. The combined trigger efficiency to select hadronic events exceeds 99.9% [8].

The selection of hadronic events is based on the energy measured in the electromagnetic and hadronic calorimeters. Events are accepted if:

$$0.6 < \frac{E_{\rm vis}}{\sqrt{s}} < 1.4 \quad , \quad \frac{|\,E_{\parallel}\,|}{E_{\rm vis}} < 0.40 \quad , \quad \frac{E_{\perp}}{E_{\rm vis}} < 0.40 \quad , \quad N_{cluster} > 12,$$

where $E_{\rm vis}$ is the total energy observed in the calorimeters, $E_{\parallel}$ is the energy imbalance along the beam direction, and $E_{\perp}$ is the transverse energy imbalance. An algorithm is used to group into clusters, neighbouring calorimeter signals, which are likely to be produced by the same particle. Only clusters with a total energy above 100 MeV are used. The number of clusters produced is approximately proportional to the number of particles in the event, so the cut on the number of clusters rejects low multiplicity non-hadronic events. Applying the same cuts to simulated events, we find that 98% of the hadronic decays from the Z^0 are accepted.

In order to reduce the contribution from initial state photons and interference between initial and final state radiation, we limit our study to hadronic events detected near the peak of the Z^0 resonance, in the center of mass energy range 91.0 GeV $< \sqrt{s} <$ 91.5 GeV. We collected 323 674 of such events.

While jets are reconstructed in the angular region $5^\circ < \theta < 175^\circ$, photon candidates are selected only from the barrel region of the electromagnetic detector ($45^\circ < \theta < 135^\circ$), where the contribution from initial state radiation is minimal.

For efficiency and background studies we use $\sim$ 890 000 Monte-Carlo events generated using JETSET with parton shower and string fragmentation. We also use $\sim$ 260 000 events, generated with HERWIG for studies of systematic errors. The two samples have been passed through the full L3 detector simulation [9].

The main background to final state radiation is due to π^0's and η's decaying into photons. Since these mesons tend to have a relatively low energy and are emitted close to the direction of the jets, the ratio of the direct photon signal with respect to the background is enhanced when looking for high energy, isolated neutral electromagnetic clusters.

We define photon candidates as clusters in the central electromagnetic calorimeter with an energy $E > 5$ GeV, and with no charged track within a region $\delta\phi = \pm 1.15^\circ$ in the plane perpendicular to the beam axis. We eliminate part of the background by requiring no other electromagnetic clusters, with an energy above 500 MeV in a cone of half-angle $\xi_c = 15^\circ$ around the candidate direction.

Such isolation criteria are sensitive to the presence of jet fragments inside the isolation cone. In order to check the accuracy of Monte-Carlo generators in simulating the inter-jet fragmentation two methods have been applied: 1) the measurement of the isolation of randomly generated vectors in hadronic events [10] and 2) the counting of the multiplicity of low energy

calorimetric clusters between jets. We find that the generators JETSET and HERWIG, after full detector simulation, correctly reproduce the low energy inter-jet activity under the following conditions:

- The isolation is conservatively defined with respect to clusters having an energy greater than 500 MeV. A lower energy threshold of 100-200 MeV would be more suitable for background rejection, but with such a threshold, the Monte-Carlo simulations JETSET and HERWIG do not fully agree with each other and with the data. From the study of random beam gate triggers and from the comparison of JETSET and HERWIG with data we conclude that the disagreement is not due to an imprecise detector simulation. The disagreement is therefore attributed to inaccuracies of the Monte Carlo models in describing the production of low energy particles in the inter-jet region. We emphasize here that the observed differences are specific to the inter-jet region, i.e. no significant discrepancy is observed for the overall multiplicity of clusters with energy above 100 MeV.

- The isolated objects must be separated by more than 20° from the axis of each jet. The special configuration where an object is close to a jet axis, yet is isolated with respect to other electromagnetic clusters, is not correctly reproduced by the simulation.

For each selected event, we form jets using the JADE algorithm [11] with the parameter $y_{cut} = 0.05$, excluding in turn each photon candidate from the reconstruction. We keep events containing at least one photon candidate which is isolated by more than $\xi_j = 20°$ from the axis of each jet.

After the above cuts, we are left with 3202 events of which 31 include more than one direct photon candidate. Using JETSET, the efficiency for selecting final state photons in our geometrical acceptance, which have $E_\gamma > 5$ GeV and which are isolated by more than 20° from the axis of each jet, is estimated at 80%.

The initial state radiation background in our sample has been estimated to be 69 ± 5 events using JETSET. Because this generator has initial state radiation implemented only to first order, we have used a different generator (BHAGENE [12]) to estimate a contribution of –15 events from higher order corrections. This number will be used as a contribution to our systematic error. The initial state contribution will always be subtracted in the following analysis. The $Z^0 \rightarrow \tau^+\tau^-(\gamma)$ background is estimated, using the KORALZ 3.8 [13] event generator, to be less than $\simeq 0.5\%$ of the selected event sample and is therefore neglected.

4 Background Estimation and Final State Photon Yield

After the previous selection has been applied, the remaining background is due to neutral hadrons occurring either as single isolated particles or in tight groups of particles which decay into adjacent photons. The Monte-Carlo simulation indicates that the background decreases very fast when the energy cut increases, but also that a tail is still present up to 45 GeV. It is important to note that we are exploring a peripheral region of the jets where fragmentation models are not very reliable, in particular for energies above 5 GeV. Hence, it is not possible to directly subtract the background using Monte-Carlo events. In order to minimize the use of the Monte-Carlo, we determine whether or not an electromagnetic cluster is a single photon by studying the transverse shower profile in the electromagnetic calorimeter.

For each candidate we compute the function:

$$C = \frac{1}{N}\sum_i \omega_i(E_i)[\mathcal{E}_i(\theta_0,\phi_0,W_0) - E_i]^2$$

where E_i is the energy observed in crystal i, $i = 1,...,N$, N is the number of crystals with an energy deposit in the cluster and $\mathcal{E}_i(\theta_0,\phi_0,W_0)$ is the energy that would be deposited in crystal i by a single photon of energy W_0 hitting the calorimeter at position (θ_0,ϕ_0), as predicted by the detector simulation program GEANT 3.14 [9]. The weighting function, $\omega_i(W_0)$, associated with the energy fluctuations in crystal i for a single photon of energy W_0, is chosen to optimize the sensitivity of the algorithm in discriminating single photon showers from multi-photon ones[1)]. The C function is minimized with respect to the parameters θ_0, ϕ_0 and W_0, and the minimum value of C is used as a parameter to discriminate between single and multiple photon showers.

By comparing electron and photon showers produced by our Monte-Carlo simulation with data from radiative dilepton Z^0 decays, we find that the C distributions agree in width and position to within 5%. We also observe that the C distribution for photons is nearly energy independent above 5 GeV.

In Table 1 we show the algorithm's ability to reject π^0 mesons, choosing a cut, $C < 40$. We also indicate the corresponding photon identification efficiency.

π^0 energy (GeV)	π^0 rejection power (%)	Efficiency for γ (%)
5	90 ± 3 (stat)	92.0 ± 0.5 (stat)
10	92 ± 2	93.5 ± 0.5
15	72 ± 2	94.0 ± 0.5
20	46 ± 2	93.5 ± 0.5
25	29 ± 1	94.0 ± 0.5
30	20 ± 1	92.5 ± 0.5
35	15 ± 1	92.0 ± 0.5
45	11 ± 1	90.5 ± 0.5

Table 1: Shower shape rejection power for π^0 as a function of the energy and corresponding photon identification efficiency for $C < 40$.

In Fig. 1a, we show the C distribution for the selected events with $C < 300$, together with the predictions from JETSET. 90% of the signal from single photons is contained in the peak below $C = 40$. The Monte-Carlo simulation indicates that the background from single neutral hadrons (mostly π^0) has a distribution concentrated predominantly in the low part of the C spectrum. The JETSET phenomenology indicates that these "single" π^0 are mostly a direct product of string fragmentation; the selection of this component from JETSET events displays a peak at low C with a long tail. In contrast, decay products of heavier mesons can have many particles in the final state and we find that the electromagnetic clusters associated with these events give a flatter C distribution. With our isolation criteria, the magnitude of the "string" and "decay" components in the unmodified generator is almost identical.

The signal yield can be estimated by a two-parameter fit of the predicted single photon and

[1]Compared to a standard χ^2 calculation, we found that a better sensitivity is obtained by giving larger weights to the 8 crystals surrounding the central one.

background shapes to the data in the form:

$$D = S \cdot R_s + B \cdot R_b \tag{1}$$

where D represents the data and S (B) is the Monte-Carlo distribution for signal (background) normalized to the total number of hadronic events. R_s and R_b are free parameters of the fit. We perform the fit in the region $C < 120$ which includes all the signal and minimizes the sensitivity to the multi-hadron contribution from decay chains. The fit, shown in Fig. 1b, yields a signal of 848 ± 55 events, which corresponds to a ratio between data and JETSET for the single photon yield of

$$R_s = 1.14 \pm 0.06,$$

where the error is statistical only and accounts for both the data and Monte-Carlo contributions. The fit gives a χ^2 of 80 for 98 degrees of freedom, and the result changes by less than 2% when varying the fit region from $0 < C < 80$ to $0 < C < 140$. The background is underestimated in JETSET by the factor $R_b = 1.88 \pm 0.08$ (stat).

The main systematic error is associated with the background subtraction. We now discuss this topic in more detail.

The fit tends to overestimate the background contribution in the region $C > 150$ by about 20%. This can be interpreted as a mistuning of the "string" component of the background (containing most of the "single" π^0's) relative to the component from decay chains. In order to estimate the effect of this mistuning on the results of fit (1), we add an extra degree of freedom to our fit by allowing for a single π^0 yield different from the standard JETSET prediction.

The three parameter fit:

$$D = S \cdot R_s + B \cdot R_b + B_{\pi^0} \cdot R_{\pi^0} \tag{2}$$

takes into account the C distribution, predicted for a component of isolated single π^0's: B_{π^0}. The distribution B_{π^0} is a function of the π^0 energy spectrum. The latter is estimated as follows. The Monte-Carlo background is scaled up by a factor 1.6 so as to fit the data for $C > 160$. The excess of data over Monte-Carlo for $C < 120$ is interpreted as isolated single π^0's and their energy spectrum in this region is estimated by subtracting the scaled Monte-Carlo energy distribution from the data. The corresponding C distribution is denoted by B_{π^0} in equation (2). The result of a global fit (2) ($0 < C < 300$) is $R_s = 1.09 \pm 0.07$(stat), with the extra π^0's accounting for $\approx 30\%$ of the total background. We interpret the 0.05 deviation from fit (1) as a consequence of the mistuning of the two components of background in JETSET and we use this result as an estimate of the associated systematic error.

Two possible origins of this discrepancy in the background composition beween data and JETSET were investigated in some detail [14]: a) small non-gaussian tails in the distribution of intrinsic $p_\perp$ introduced during fragmentation. This hypothesis has been tested by doubling the $\sigma_{p_\perp}$ for a fraction f of the particles generated in the string fragmentation. We found that a factor two increase in the isolated background can be achieved for $f \sim 1.3\%$. b) a reduction in the light vector meson yield in the string fragmentation, compared to pseudoscalar meson production, also enhances the isolated component. Given the rather crude experimental knowledge of the peripheral region of the fragmentation process associated with our background, we are unable to exclude either of these two possibilities.

As a further study of the systematic error, we note that the C parameter cannot distinguish π^0's from single photons at energies above $\sim$ 30 GeV, so we have been implicitly using JETSET to extrapolate the background subtraction at higher energy. Figure 2 shows the measured

energy distribution for data and JETSET after a cut $C < 40$. The background predicted by JETSET has been rescaled by the factor 1.88 and contains 60 events for $E > 30$ GeV. A similar analysis of HERWIG events gives only 25 events in this region. We translate this difference into an error on R_s of ± 0.04.

Since the angular isolation cuts and shower shape analyses both contribute to the background rejection in independent ways, we can estimate another contribution to the systematic error by changing the angular cuts and therefore leaving different amounts of background to be rejected by the shower shape analysis. We check the stability of the ratio R_s by varying ξ_c from 20° down to the size of an electromagnetic cluster of $\sim 5°$ and find variations of ± 0.04.

Other contributions to the systematic error in the value of R_s are: a) inaccuracies in the shower shape modeling, b) imprecision in the association of charged tracks and showers in the electromagnetic calorimeter, and c) differences in signal acceptance due to the fragmentation model. To check the first point, the Monte-Carlo C distribution, which was found to reproduce the data within 1 unit in position and r.m.s., is shifted and smeared by 1 unit, around the nominal position. The fit is performed again, resulting in a change of less than ± 0.02 in the value of R_s. The second point is checked by allowing $\delta\phi$ to vary according to the relative resolution of the two detectors, giving a contribution of ± 0.02. Finally, the last point is checked by comparing the signal acceptance obtained by JETSET with that from HERWIG (see section 5), resulting in a contribution of ± 0.02 to the systematic error.

We estimate the total systematic error on R_s as the quadratic sum of the contributions previously discussed (see Table 2).

item	default	range of change	error on R_s
Fit with extra-π^0			± 0.05
Choice of C fit region	< 120	< 80 or < 140	± 0.02
Extrapolation backg. $E > 30$ GeV			± 0.04
Shower shape agreement Data-MC			± 0.02
ξ_c	15°	5-20	± 0.04
$\delta\phi$	1.15°	1.03-1.26	± 0.01
Acceptance JETSET-HERWIG			± 0.02
Initial State Radiation			± 0.02

Table 2: Systematic contributions to the error on the measurement of the direct photon rate

As a first cross-check to our background estimate, we perform a direct reconstruction of isolated π^0 and η mesons. In hadronic events, we select pairs of clusters in the electromagnetic calorimeter. Each cluster must have an energy of at least 500 MeV and should be isolated by more than $\delta\phi = 1.15°$ from any charged tracks. We then apply the previously described energy and isolation cuts used for the photon selection, to the system formed by the two clusters.

The invariant mass distribution of the cluster pairs in the π^0 (η) region is plotted in Fig. 3a (Fig. 3b). By fitting two gaussians plus a smooth background shape, we find for the ratio between data and JETSET:

$$R_{\pi^0} = 1.84 \pm 0.12\,(\text{stat}) \quad ; \quad \mathrm{R}_\eta = 2.11 \pm 0.22\,(\text{stat}).$$

We use these factors to rescale the JETSET predictions shown in Fig. 3.

Due to the angular resolution of the electromagnetic calorimeter, we are unable to reconstruct the mass of high energy π^0 mesons and it is not possible by this method to estimate the background due to neutral hadrons in the full energy spectrum. Nevertheless, since the background is concentrated at low energy (Fig. 2), we conclude that this cross-check is consistent with our previous background estimate.

Since most of the charged tracks observed in the detector are $\pi^{\pm}$ and most of our background arises from π^0, isospin symmetry can be used to further cross-check the background estimate by comparing the production rate of isolated charged hadrons in the data and in Monte-Carlo simulation. We therefore search for charged tracks that fulfill the same energy and isolation criteria applied to the neutral candidates. While the systematics of this selection differ somewhat from those of the neutral search, we find a similar discrepancy in the comparison of data to Monte-Carlo. The ratio of data to JETSET is found to be 1.45 ± 0.35 (stat+syst), consistent with a larger background yield than the Monte-Carlo prediction.

We note that the background discussed in this section is energetic and isolated from jets. Hence, the previous results are not in contradiction with the observation that the overall π^0 and η meson yield is well reproduced by JETSET [15,16].

Our final result for the prompt photon yield relative to JETSET is

$$R_s = 1.14 \pm 0.06(\text{stat}) \pm 0.08(\text{syst}).$$

5 Comparison with QCD

We compare our data with the three event generators after having corrected for detector effects. For each of the distributions under study, we compute a set of correction coefficients, $c(i) = d_{\text{part}}(i)/d_{\text{det}}(i)$, as the ratio of the distribution at the "particle level" (i.e. obtained by the analysis of the 4-vectors given by the generators), $d_{\text{part}}(i)$, to that at the detector level, $d_{\text{det}}(i)$, for bin i. For this purpose, we use two samples of Monte-Carlo events, generated using JETSET and HERWIG, which contain photons emitted by quarks . Each sample is equivalent to $\sim 1.2 \times 10^6$ hadronic events. For each sample we obtain $d_{\text{part}}(i)$ by applying the energy cut ($E_\gamma > 5$ GeV) and the cut on the isolation to the closest jet ($\xi_j = 20°$), while the distribution $d_{\text{det}}(i)$ is computed using events simulated in the L3 detector to which the full set of cuts, described in section 3, has been applied along with a cut requiring $C < 40$. We find small differences of the order of 4% between the coefficients $c(i)$ computed using the two different generators and we use the average of the two sets of coefficients to correct our data. The systematic errors on the correction procedure are taken to be half of the difference between the results obtained using the two generators. The bin size in the above distributions is chosen to be large enough to keep the bin-to-bin migration small and to avoid large statistical fluctuations.

Data distributions are obtained by applying the full set of cuts including the cut $C < 40$. The remaining neutral hadron background is then subtracted using the JETSET prediction scaled by the factor 1.88 discussed in the previous section. Initial state radiation is also removed using the Monte-Carlo prediction. In these conditions the total background contribution amounts to 35% of our data sample. Finally, the correction coefficients $c(i)$ are applied to obtain the particle-level distributions.

The branching ratio of measured Z^0 hadronic decays including photons relative to the total hadronic yield is :

$$\text{BR}(Z^0 \to \text{hadrons} + \gamma)/\text{BR}(Z^0 \to \text{hadrons}) = [5.2 \pm 0.3(\text{stat}) \pm 0.4(\text{syst})] \cdot 10^{-3}$$

for a photon energy cut of 5 GeV and an isolation of the photon with respect to the closest jet of at least 20°. The jets are defined by the JADE algorithm with $y_{cut} = 0.05$, as discussed previously.

The Monte Carlo predicted branching ratios, with identical analysis conditions, are:

$$\begin{aligned} \text{JETSET}: &\quad [4.53 \pm 0.04\,(\text{stat})] \cdot 10^{-3} \\ \text{HERWIG}: &\quad [6.09 \pm 0.04\,(\text{stat})] \cdot 10^{-3} \\ \text{ARIADNE}: &\quad [6.13 \pm 0.04\,(\text{stat})] \cdot 10^{-3} \end{aligned}$$

Figure 4 shows the comparison of our data with the three QCD calculations for the distributions of: a) the photon energy, b) the angle to the closest jet, and c) the transverse energy with respect to the event thrust axis (calculated with the photon). The Monte Carlo distributions are obtained from a sample of 3×10^6 hadronic events for each generator, using parameters obtained from a global tuning of hadronic event shapes to data [17].

Although the precision of our measurement does not allow us to discriminate between the models we observe a qualitatively good agreement between data and the prediction of the Monte Carlo programs. However differences between models in the 30% range can be explained considering the necessary extrapolation from the soft and collinear limit where the approach is strictly applicable. The fact that we do not observe stronger discrepancies between the models is probably due to a forced matching, in all models, of the first branch to the $\mathcal{O}(\alpha)$ matrix element. Tests of some of the above QCD calculations have been already reported by other Collaborations at LEP [10,18–20].

6 Search for New Processes

Our sample of events with one or two hard isolated photons can be used to search for new processes involving photon emission. For this part of the analysis, we employ the same cuts as described above, including $C < 40$. We consider:

(a) Z^0 radiative decay to a narrow resonance, Y, which subsequently decays into hadrons: $Z^0 \to Y\gamma$ with $Y \to$ hadrons.

(b) Production of one or two excited quarks, which decay radiatively: $Z^0 \to q^*q^*$ and $Z^0 \to q^*q$ with $q^* \to q\gamma$.

(c) Production of a scalar boson, S, which decays into two photons: $Z^0 \to S +$ hadrons with $S \to \gamma\gamma$.

Cases (a) and (c) are also signatures for Higgs production. Limits for the first two processes have been previously published [21,18,22,19].

In the case of the Z^0 decaying radiatively to a narrow high mass resonance, the signature expected is a monochromatic photon plus jets. We make use of the high precision photon energy measurement of the L3 detector to determine the mass of the particles recoiling against the photon. The resolution of the recoil mass is determined from the photon energy resolution and is better than 2% for $M_Y > 50$ GeV. We scan the data for a peak in the recoil mass spectrum using a mass window given by $\Delta M_Y = 0.03(s - M_Y^2)/M_Y$ [22]. The bin size, ΔM_Y, is chosen so that more than 80% of the signal from a narrow resonance is confined to a single bin in the recoil mass spectrum. The background is estimated by fitting a smooth curve to the data, thus avoiding the uncertainties coming from Monte-Carlo background predictions. We find

no statistically significant excess. The acceptance of our cuts, as determined from the signal Monte-Carlo, varies from 33% at M_Y=35 GeV to 24% at M_Y=85 GeV. The 95% confidence level upper limit on $\sigma(e^+e^- \to Z^0 \to Y\gamma) \times BR(Y \to \text{hadrons})$ is shown in Fig. 5a. This result significantly improves our previous limit [22].

The existence of excited quarks is a natural consequence of various composite models [23]. Excited quarks can be produced singly or in pairs. In the pair production case, only q^* with masses smaller than the beam energy can be produced, while in the single production case we can search for q^* with masses up to $M_{q^*} \leq M_Z - M_q$. To study the production of a pair of excited quarks, we search for events with two photons passing our cuts. We find 4 events in the data. The acceptance, calculated from a Monte-Carlo generator [24] based on the differential cross section in [25], varies between 21% and 36% for $M_{q^*} > 15$ GeV depending on the q^* mass. No background has been subtracted, thus, we obtain a 95% confidence level upper limit of $\sigma(e^+e^- \to Z^0 \to q^*q^*) \times BR^2(q^* \to q\gamma) < 2$ pb. Assuming standard fermion couplings to the Z^0 [26] and using all 5 flavours, the production cross section can be calculated and we extract a limit on $BR(q^* \to q\gamma) < 4\%$ for M_{q^*} up to 45 GeV.

To investigate single q^* production, we search for a peak in the γ-jet invariant mass spectrum, considering only those events which are made up of a photon and exactly two hadronic jets. The γ-jet invariant mass resolution is improved by imposing the constraints of energy and momentum conservation upon each event. The improvement comes from using the accurate photon energy and the relatively well-measured jet angles to determine the jet energies. Monte-Carlo simulations [24, 27] predict a γ-jet invariant mass resolution better than 2 GeV, independent of M_{q^*}. We use a bin size of 4 GeV to scan for a peak in the γ-jet invariant mass spectrum. As in the narrow resonance case, the background is estimated from a fit to the data. The acceptance, calculated from the signal Monte-Carlo and including the 4 GeV binning efficiency, varies with q^* mass from 27% at 80 GeV to 41% at 50 GeV. This gives a 95% confidence level upper limit on $\sigma(e^+e^- \to Z^0 \to q^*q) \times BR(q^* \to q\gamma) < 10$ pb, which is shown as a function of M_{q^*} in Fig. 5b (dotted line).

Finally, we consider the possibility of Z^0 decay into a scalar boson, S, which subsequently decays into two photons. As a model to study the acceptance of our analysis, we identify S with the Higgs boson, H^0. In the Standard Model, the Higgs cannot couple to photons at tree level; however, the $H^0 \to \gamma\gamma$ decay can proceed via one-loop diagrams involving charged fermions and W bosons. As mentioned above, we have found 4 events with a pair of final-state photons. We use the PYTHIA 5.6 Monte-Carlo [28] to simulate Higgs events with the Higgs decaying into two photons. The acceptance varies from 19% to 35% in the range 10 GeV $< M_H <$ 70 GeV. The $\gamma\gamma$ invariant mass resolution is $\approx 6\%$ for M_H=10 GeV and is better than 2% for $M_H > 30$ GeV. Using this estimate for the resolution, we find that the 4 events falling in the mass region explored, appear in different $\gamma\gamma$ invariant mass bins. No background has been subtracted, leading to the conservative 95% confidence level upper limit for $\sigma(e^+e^- \to H^0 + \text{hadrons}) \times BR(H^0 \to \gamma\gamma)$ which is plotted as a function of M_H in Fig. 5b (solid line). The limit is still several orders of magnitude above the Standard Model prediction.

7 Conclusions

We have studied the production of direct photons in hadronic Z^0decays. We have found that the background due to isolated, energetic neutral hadrons decaying into photons is underestimated in JETSET by a factor of almost 2. After background subtraction, we measure the branching

ratio for direct photon events relative to the total hadron production to be:

$$\mathrm{BR}(Z^0 \to \mathrm{hadrons} + \gamma)/\mathrm{BR}(Z^0 \to \mathrm{hadrons}) = [5.2 \pm 0.3(\mathrm{stat}) \pm 0.4(\mathrm{syst})] \cdot 10^{-3}$$

where a 5 GeV photon energy cut and an isolation of 20° with respect to the closest jet have been considered. The main contribution to the systematic error is associated with the uncertainty in the background subtraction.

We have also compared the distributions of the photon energy, its transverse energy with respect to the event thrust and its angle to the jet axis, to the predictions of three QCD leading logarithm calculations. The differences between the models are of the order of 30%. With the accuracy of the analysis, we observe a good general agreement between our measurements and the model predictions and we cannot discriminate between them.

We have also used our data set to search for new processes involving hard photons, we find no evidence for processes beyond the Standard Model and we have set limits for the reactions: $Z^0 \to Y\gamma$ with $Y \to$ hadrons, $Z^0 \to q^*q^*$, $Z^0 \to q^*q$ with $q^* \to q\gamma$ and $Z^0 \to S +$ hadrons with $S \to \gamma\gamma$.

8 Acknowledgements

We express our gratitude to the CERN accelerator divisions for the excellent performance of the LEP machine. We acknowledge the effort of all engineers and technicians who have participated in the construction and maintenance of this experiment.

We wish to thank T. Sjöstrand for many helpful discussions.

The L3 Collaboration:

O.Adriani,[14] M.Aguilar-Benitez,[23] S.Ahlen,[9] H.Akbari,[5] J.Alcaraz,[15] A.Aloisio,[25] G.Alverson,[10] M.G.Alviggi,[25] G.Ambrosi,[30] Q.An,[16] H.Anderhub,[43] A.L.Anderson,[13] V.P.Andreev,[34] T.Angelov,[13] L.Antonov,[38] D.Antreasyan,[7] P.Arce,[23] A.Arefiev,[24] A.Atamanchuk,[34] T.Azemoon,[3] T.Aziz,[8,1] P.V.K.S.Baba,[16] P.Bagnaia,[33] J.A.Bakken,[32] L.Baksay,[39] R.C.Ball,[3] S.Banerjee,[8] J.Bao,[5] R.Barillère,[15] L.Barone,[33] R.Battiston,[30] A.Bay,[17] F.Becattini,[14] U.Becker,[13,43] F.Behner,[43] J.Behrens,[43] S.Beingessner,[4] Gy.L.Bencze,[11] J.Berdugo,[23] P.Berges,[13] B.Bertucci,[30] B.L.Betev,[38,43] M.Biasini,[30] A.Biland,[43] G.M.Bilei,[30] R.Bizzarri,[33] J.J.Blaising,[4] B.Blumenfeld,[5] G.J.Bobbink,[15,2] M.Bocciolini,[14] R.Bock,[1] A.Böhm,[1] B.Borgia,[33] D.Bourilkov,[27] M.Bourquin,[17] D.Boutigny,[4] B.Bouwens,[2] E.Brambilla,[25] J.G.Branson,[35] I.C.Brock,[31] M.Brooks,[21] C.Buisson,[22] A.Bujak,[40] J.D.Burger,[13] W.J.Burger,[17] J.P.Burq,[22] J.Busenitz,[39] X.D.Cai,[16] M.Capell,[20] M.Caria,[30] G.Carlino,[25] F.Carminati,[14] A.M.Cartacci,[14] M.Cerrada,[23] F.Cesaroni,[33] Y.H.Chang,[13] U.K.Chaturvedi,[16] M.Chemarin,[22] A.Chen,[45] C.Chen,[6] G.M.Chen,[6] H.F.Chen,[18] H.S.Chen,[6] J.Chen,[13] M.Chen,[13] M.L.Chen,[3] W.Y.Chen,[16] G.Chiefari,[25] C.Y.Chien,[5] M.Chmeissani,[3] S.Chung,[13] C.Civinini,[14] I.Clare,[13] R.Clare,[13] T.E.Coan,[21] H.O.Cohn,[28] G.Coignet,[4] N.Colino,[15] A.Contin,[7] F.Crijns,[27] X.T.Cui,[16] X.Y.Cui,[16] T.S.Dai,[13] R.D'Alessandro,[14] R.de Asmundis,[25] A.Degré,[4] K.Deiters,[13] E.Dénes,[11] P.Denes,[32] F.DeNotaristefani,[33] M.Dhina,[43] D.DiBitonto,[39] M.Diemoz,[33] H.R.Dimitrov,[38] C.Dionisi,[33,15] M.T.Dova,[16] E.Drago,[25] T.Driever,[27] D.Duchesneau,[17] P.Duinker,[2] I.Duran,[36] H.El Mamouni,[22] A.Engler,[31] F.J.Eppling,[13] F.C.Erné,[2] P.Extermann,[17] R.Fabbretti,[41] M.Fabre,[41] S.Falciano,[33] S.J.Fan,[37] O.Fackler,[20] J.Fay,[22] M.Felcini,[15] T.Ferguson,[31] D.Fernandez,[23] G.Fernandez,[23] F.Ferroni,[33] H.Fesefeldt,[1] E.Fiandrini,[30] J.Field,[17] F.Filthaut,[27] G.Finocchiaro,[33] P.H.Fisher,[5] G.Forconi,[17] T.Foreman,[2] K.Freudenreich,[43] W.Friebel,[42] M.Fukushima,[13] M.Gailloud,[19] Yu.Galaktionov,[24,13] E.Gallo,[14] S.N.Ganguli,[8] P.Garcia-Abia,[23] S.S.Gau,[45] D.Gele,[22] S.Gentile,[33,15] S.Goldfarb,[10] Z.F.Gong,[18] E.Gonzalez,[23] P.Göttlicher,[1] A.Gougas,[5] D.Goujon,[17] G.Gratta,[29] C.Grinnell,[13] M.Gruenewald,[29] C.Gu,[16] M.Guanziroli,[16] J.K.Guo,[37] V.K.Gupta,[32] A.Gurtu,[15,8] H.R.Gustafson,[3] L.J.Gutay,[40] K.Hangarter,[1] A.Hasan,[16] D.Hauschildt,[2] C.F.He,[37] T.Hebbeker,[1] M.Hebert,[35] G.Herten,[13] U.Herten,[1] A.Hervé,[15] K.Hilgers,[1] H.Hofer,[43] H.Hoorani,[17] G.Hu,[16] G.Q.Hu,[37] B.Ille,[22] M.M.Ilyas,[16] V.Innocente,[15,25] H.Janssen,[15] S. Jezequel,[4] B.N.Jin,[6] L.W.Jones,[3] A.Kasser,[19] R.A.Khan,[16] Yu.Kamyshkov,[28] P.Kapinos,[34,42] J.S.Kapustinsky,[21] Y.Karyotakis,[15,4] M.Kaur,[16] S.Khokhar,[16] M.N.Kienzle-Focacci,[17] W.W.Kinnison,[21] D.Kirkby,[29] S.Kirsch,[42] W.Kittel,[27] A.Klimentov,[13,24] A.C.König,[27] E.Koffeman,[2] O.Kornadt,[1] V.Koutsenko,[13,24] A.Koulbardis,[34] R.W.Kraemer,[31] T.Kramer,[13] V.R.Krastev,[38,30] W.Krenz,[1] A.Krivshich,[34] H.Kuijten,[27] K.S.Kumar,[12] A.Kunin,[12,24] G.Landi,[14] D.Lanske,[1] S.Lanzano,[25] P.Lebrun,[22] P.Lecomte,[43] P.Lecoq,[15] P.Le Coultre,[43] D.M.Lee,[21] I.Leedom,[10] J.M.Le Goff,[15] R.Leiste,[42] M.Lenti,[14] E.Leonardi,[33] J.Lettry,[43] X.Leytens,[2] C.Li,[18,16] H.T.Li,[6] P.J.Li,[37] X.G.Li,[6] J.Y.Liao,[37] W.T.Lin,[45] Z.Y.Lin,[18] F.L.Linde,[15,2] B.Lindemann,[1] D.Linnhofer,[43] L.Lista,[25] Y.Liu,[16] W.Lohmann,[42,15] E.Longo,[33] Y.S.Lu,[6] J.M.Lubbers,[15] K.Lübelsmeyer,[1] C.Luci,[33] D.Luckey,[7,13] L.Ludovici,[33] L.Luminari,[33] W.Lustermann,[42] J.M.Ma,[6] W.G.Ma,[18] M.MacDermott,[43] P.K.Malhotra,[8] † R.Malik,[16] A.Malinin,[4,24] C.Maña,[23] D.N.Mao,[3] Y.F.Mao,[6] M.Maolinbay,[43] P.Marchesini,[43] F.Marion,[4] A.Marin,[9] J.P.Martin,[22] L.Martinez-Laso,[23] F.Marzano,[33] G.G.G.Massaro,[2] T.Matsuda,[13] K.Mazumdar,[8] P.McBride,[12] T.McMahon,[40] D.McNally,[43] Th.Meinholz,[1] M.Merk,[27] L.Merola,[25] M.Meschini,[14] W.J.Metzger,[27] Y.Mi,[16] G.B.Mills,[21] Y.Mir,[16] G.Mirabelli,[33] J.Mnich,[1] M.Möller,[1] B.Monteleoni,[14] R.Morand,[4] S.Morganti,[33] N.E.Moulai,[16] R.Mount,[29] S.Müller,[1] A.Nadtochy,[34] E.Nagy,[11] M.Napolitano,[25] H.Newman,[29] C.Neyer,[43] M.A.Niaz,[16] A.Nippe,[1] H.Nowak,[42] G.Organtini,[33] D.Pandoulas,[1] S.Paoletti,[14] P.Paolucci,[25] G.Passaleva,[14,30] S.Patricelli,[25] T.Paul,[5] M.Pauluzzi,[30] F.Pauss,[43] Y.J.Pei,[1] D.Perret-Gallix,[4] J.Perrier,[17] A.Pevsner,[5] D.Piccolo,[25] M.Pieri,[15,14] P.A.Piroué,[32] F.Plasil,[28] V.Plyaskin,[24] M.Pohl,[43] V.Pojidaev,[24,14] N.Produit,[17] J.M.Qian,[3] K.N.Qureshi,[16] R.Raghavan,[8] G.Rahal-Callot,[43] G.Raven,[2] P.Razis,[26] K.Read,[28] D.Ren,[43] Z.Ren,[16] M.Rescigno,[33] S.Reucroft,[10] A.Ricker,[1] S.Riemann,[42] O.Rind,[3] H.A.Rizvi,[16] F.J.Rodriguez,[23] B.P.Roe,[3] M.Röhner,[1] S.Röhner,[1] L.Romero,[23] J.Rose,[1] S.Rosier-Lees,[4] R.Rosmalen,[27] Ph.Rosselet,[19] A.Rubbia,[13] J.A.Rubio,[15] H.Rykaczewski,[43] M.Sachwitz,[42] E.Sajan,[30] J.Salicio,[15] J.M.Salicio,[23] G.S.Sanders,[21] A.Santocchia,[30] M.S.Sarakinos,[13] G.Sartorelli,[7,16] M.Sassowsky,[1] G.Sauvage,[4] V.Schegelsky,[34] K.Schmiemann,[1] D.Schmitz,[1] P.Schmitz,[1] M.Schneegans,[4] H.Schopper,[44] D.J.Schotanus,[27] S.Shotkin,[13] H.J.Schreiber,[42] J.Shukla,[31] R.Schulte,[1] S.Schulte,[1] K.Schultze,[1] J.Schütte,[12] J.Schwenke,[1] G.Schwering,[1] C.Sciacca,[25] I.Scott,[12] R.Sehgal,[16] P.G.Seiler,[41] J.C.Sens,[15,2] L.Servoli,[30] I.Sheer,[35] D.Z.Shen,[37] S.Shevchenko,[29] X.R.Shi,[29] E.Shumilov,[24] V.Shoutko,[24] E.Soderstrom,[32] A.Sopczak,[35] C.Spartiotis,[5] T.Spickermann,[1] P.Spillantini,[14] R.Starosta,[1] M.Steuer,[7,13] D.P.Stickland,[32] F.Sticozzi,[13] H.Stone,[17] K.Strauch,[12] B.C.Stringfellow,[40] K.Sudhakar,[8,1] G.Sultanov,[16] R.L.Sumner,[32] L.Z.Sun,[18,16] H.Suter,[43] R.B.Sutton,[31] J.D.Swain,[16] A.A.Syed,[16] X.W.Tang,[6] L.Taylor,[10] C.Timmermans,[27] Samuel C.C.Ting,[13] S.M.Ting,[13] M.Tonutti,[1] S.C.Tonwar,[8] J.Tóth,[11] A.Tsaregorodtsev,[34] G.Tsipolitis,[31] C.Tully,[29] K.L.Tung,[6] J.Ulbricht,[43] L.Urbán,[11] U.Uwer,[1] E.Valente,[33] R.T.Van de Walle,[27] I.Vetlitsky,[24] G.Viertel,[43] P.Vikas,[16] U.Vikas,[16] M.Vivargent,[4] H.Vogel,[31] H.Vogt,[42] I.Vorobiev,[24] A.A.Vorobyov,[34] L.Vuilleumier,[19] M.Wadhwa,[16] W.Wallraff,[1] C.R.Wang,[18] G.H.Wang,[31] J.H.Wang,[6] Q.F.Wang,[12] X.L.Wang,[18] Y.F.Wang,[14] Z.M.Wang,[16,18] A.Weber,[1] J.Weber,[43] R.Weill,[19] T.J.Wenaus,[20] J.Wenninger,[17] M.White,[13] C.Willmott,[23] F.Wittgenstein,[15] D.Wright,[32] R.J.Wu,[6] S.X.Wu,[16] Y.G.Wu,[6] B.Wysłouch,[13] Y.Y.Xie,[37] Y.D.Xu,[6] Z.Z.Xu,[18] Z.L.Xue,[37] D.S.Yan,[37] X.J.Yan,[13] B.Z.Yang,[18] C.G.Yang,[6] G.Yang,[16] K.S.Yang,[6] Q.Y.Yang,[6] Z.Q.Yang,[37] C.H.Ye,[16] J.B.Ye,[18] Q.Ye,[16] S.C.Yeh,[45] Z.W.Yin,[37] J.M.You,[16] N.Yunus,[16] M.Yzerman,[2] C.Zaccardelli,[29] P.Zemp,[43] M.Zeng,[16] Y.Zeng,[1] D.H.Zhang,[2] Z.P.Zhang,[18,16] B.Zhou,[9] J.F.Zhou,[1] R.Y.Zhu,[29] H.L.Zhuang,[6] A.Zichichi,[7,15,16] B.C.C.van der Zwaan[2]

1 I. Physikalisches Institut, RWTH, W-5100 Aachen, FRG[§]
III. Physikalisches Institut, RWTH, W-5100 Aachen, FRG[§]
2 National Institute for High Energy Physics, NIKHEF, NL-1009 DB Amsterdam, The Netherlands
3 University of Michigan, Ann Arbor, MI 48109, USA
4 Laboratoire d'Annecy-le-Vieux de Physique des Particules, LAPP,IN2P3-CNRS, BP 110, F-74941 Annecy-le-Vieux CEDEX, France
5 Johns Hopkins University, Baltimore, MD 21218, USA
6 Institute of High Energy Physics, IHEP, Beijing, P.R. China
7 INFN-Sezione di Bologna, I-40126 Bologna, Italy
8 Tata Institute of Fundamental Research, Bombay 400 005, India
9 Boston University, Boston, MA 02215, USA
10 Northeastern University, Boston, MA 02115, USA
11 Central Research Institute for Physics of the Hungarian Academy of Sciences, H-1525 Budapest 114, Hungary
12 Harvard University, Cambridge, MA 02139, USA
13 Massachusetts Institute of Technology, Cambridge, MA 02139, USA
14 INFN Sezione di Firenze and University of Florence, I-50125 Florence, Italy
15 European Laboratory for Particle Physics, CERN, CH-1211 Geneva 23, Switzerland
16 World Laboratory, FBLJA Project, CH-1211 Geneva 23, Switzerland
17 University of Geneva, CH-1211 Geneva 4, Switzerland
18 Chinese University of Science and Technology, USTC, Hefei, Anhui 230 029, P.R. China
19 University of Lausanne, CH-1015 Lausanne, Switzerland
20 Lawrence Livermore National Laboratory, Livermore, CA 94550, USA
21 Los Alamos National Laboratory, Los Alamos, NM 87544, USA
22 Institut de Physique Nucléaire de Lyon, IN2P3-CNRS,Université Claude Bernard, F-69622 Villeurbanne Cedex, France
23 Centro de Investigaciones Energeticas, Medioambientales y Tecnologicas, CIEMAT, E-28040 Madrid, Spain
24 Institute of Theoretical and Experimental Physics, ITEP, Moscow, Russia
25 INFN-Sezione di Napoli and University of Naples, I-80125 Naples, Italy
26 Department of Natural Sciences, University of Cyprus, Nicosia, Cyprus
27 University of Nymegen and NIKHEF, NL-6525 ED Nymegen, The Netherlands
28 Oak Ridge National Laboratory, Oak Ridge, TN 37831, USA
29 California Institute of Technology, Pasadena, CA 91125, USA
30 INFN-Sezione di Perugia and Universitá Degli Studi di Perugia, I-06100 Perugia, Italy
31 Carnegie Mellon University, Pittsburgh, PA 15213, USA
32 Princeton University, Princeton, NJ 08544, USA
33 INFN-Sezione di Roma and University of Rome, "La Sapienza", I-00185 Rome, Italy
34 Nuclear Physics Institute, St. Petersburg, Russia
35 University of California, San Diego, CA 92182, USA
36 Dept. de Fisica de Particulas Elementales, Univ. de Santiago, E-15706 Santiago de Compostela, Spain
37 Shanghai Institute of Ceramics, SIC, Shanghai, P.R. China
38 Bulgarian Academy of Sciences, Institute of Mechatronics, BU-1113 Sofia, Bulgaria
39 University of Alabama, Tuscaloosa, AL 35486, USA
40 Purdue University, West Lafayette, IN 47907, USA
41 Paul Scherrer Institut, PSI, CH-5232 Villigen, Switzerland
42 DESY-Institut für Hochenergiephysik, O-1615 Zeuthen, FRG
43 Eidgenössische Technische Hochschule, ETH Zürich, CH-8093 Zürich, Switzerland
44 University of Hamburg, W-2000 Hamburg, FRG
45 High Energy Physics Group, Taiwan, ROC
§ Supported by the German Bundesministerium für Forschung und Technologie
† Deceased.

References

[1] H. Fritzsch, M. Gell-Mann and H. Leytwyler, Phys. Lett. **B 47** (1973) 365;
D.J. Gross and F. Wilczek, Phys. Rev. Lett. **30** (1973) 1343;
D.J. Gross and F. Wilczek, Phys. Rev. **D 8** (1973) 3633;
H.D. Politzer, Phys. Rev. Lett. **30** (1973) 1346;
K. Koller, T.F. Walsh and P.M. Zerwas, Z. Phys. **C 2** (1979) 197;
E. Laerman *et al.*, Nucl. Phys. **B 207** (1982) 205.

[2] MAC Collab,. H.R. Band *et al.*, Phys. Rev. Lett. **54** (1985) 95;
TASSO Collab., W. Braunschweig *et al.*, Z. Phys. **C 41** (1988) 385;
VENUS Collab., K. Abe *et al.*, Phys. Rev. Lett. **63** (1989) 1776;
JADE Collab., D.D. Pitzl *et al.*, Z. Phys. **C 46** (1990) 1.

[3] G. Kramer and B. Lampe, Phys. Lett. **B269** (1991) 401.

[4] ARIADNE 4.02;
L. Lönnblad, DESY Preprint 92-046 (1992), to be published in Comp. Phys. Comm; the program has been run with MSTA(20)=2.

[5] HERWIG 5.4;
G. Marchesini *et al.*, Comp. Phys. Comm. **67** (1992) 465;.

[6] JETSET 7.3;
T. Sjöstrand, Comp. Phys. Comm. **39** (1986) 347;
T. Sjöstrand and M. Bengtsson, Comp. Phys. Comm. **43** (1987) 367.

[7] L3 Collab., B. Adeva *et al.*, Nucl. Inst. Meth. **A 289** (1990) 35.

[8] L3 Collab., B. Adeva *et al.*, Z. Phys. **C 51** (1991) 179.

[9] The L3 detector simulation is based on GEANT Version 3.14.
See R. Brun *et al.*, "GEANT 3", CERN DD/EE/84-1 (Revised), September 1987.
The GHEISHA program (H. Fesefeldt, RWTH Aachen Report PITHA 85/02 (1985)) is used to simulate hadronic interactions.

[10] ALEPH Collab., D. Decamp *et al.*, Phys. Lett. **B 264** (1991) 476.

[11] JADE Collab, W. Bartel *et al.*, Z. Phys. **C 33** (1986) 23;
JADE Collab, S. Bethke *et al.*, Phys. Lett. **B 123** (1988) 235.

[12] J. H. Field and J. T. Reaman, technical note in preparation.

[13] S. Jadach, B. Ward and Z. Was, Comp. Phys. Comm. **66** (1991) 276.

[14] T. Sjöstrand, Private Communication.

[15] L3 Collab., B. Adeva *et al.*, Phys. Lett. **B 259** (1991) 199.

[16] L3 Collab., O. Adriani *et al.*, Measurement of Inclusive η Production in Hadronic Decays of the Z^0, Preprint CERN-PPE/92-83, CERN, 1992, submitted to Physics Letters B.

[17] L3 Collab., B. Adeva *et al.*, Studies of Hadronic Event Structure and Comparisons with QCD Models at the Z^0 Resonance, Preprint CERN-PPE/92-50, CERN, 1992.

[18] DELPHI Collab, P. Abreu *et al.*, Z. Phys. **C 53** (1992) 555.

[19] OPAL Collab, M.Z. Akrawy *et al.*, Phys. Lett. **B 246** (1990) 285.

[20] OPAL Collab, P.D. Acton *et al.*, Z. Phys. **C 54** (1992) 193.

[21] ALEPH Collab., D. Decamp *et al.*, Searches for New Particles in Z^0 decays using the ALEPH Detector, Preprint CERN-PPE/91-149, CERN, 1992.

[22] L3 Collab., B. Adeva *et al.*, Phys. Lett. **B 262** (1991) 155.

[23] F. Boudjema *et al.*, CERN 89-08 (1989) vol. 2, 188 and references therein.

[24] Y.F. Wang, Ph.D. Thesis, Univ. of Florence, 1992 (unpublished).

[25] K. Hagiwara *et al.*, Z. Phys. **C 29** (1985) 15.

[26] H. Baer *et al.*, Preprint CERN 86-02 (1986) 297;
K. Hagiwara, *op. cit.*

[27] F.A. Berends and P.H. Daverveldt, Nucl. Phys. **B 272** (1986) 131.

[28] H.U. Bengtsson and T. Sjöstrand, Comp. Phys. Comm. **46** (1987) 43.

Figure Captions

Fig. 1 (a) Distribution of the cluster shape parameter C after selection cuts.
The Monte-Carlo distributions are normalized to the total number of hadronic events in the data.
(b) Distribution of the cluster shape parameter C with JETSET fitted to data.
The Monte-Carlo predictions for the signal, the total background and the initial state radiation (ISR) background are shown.

Fig. 2 Photon energy distribution after the cut $C < 40$. The Monte-Carlo distributions are the JETSET predictions for the signal, the total background (renormalized by the factor of 1.88) and the initial state radiation (ISR) background.

Fig. 3 Invariant mass distributions for isolated cluster pairs for data and for JETSET. The Monte-Carlo has been rescaled by a factor 1.84 in the π^0 region (a), and by a factor 2.11 in the η region (b).

Fig. 4 Distributions of (a) the final state photon energy, (b) the angle between the photons and the nearest jet, and (c) the transverse energy of the photons with respect to the event thrust axis. Jets are defined using a y_{cut} of 0.05 and the event thrust is calculated including the photon. Photons are required to have energy greater than 5 GeV, and to be isolated from the nearest jet by more than 20°. Data points are corrected for detector effects. Initial state radiation, and neutral meson background are subtracted. The larger error bars show both the statistical and systematic errors added quadratically, the smaller correspond to the systematic errors only. Histograms show the predictions of the JETSET, HERWIG, and ARIADNE Monte-Carlo programs.

Fig. 5 (a) Upper limits at the 95% confidence level of $\sigma(e^+e^- \to Z^0 \to Y\gamma) \times BR(Y \to \text{hadrons})$ as a function of M_Y.
(b) Upper limits at the 95 % confidence level of: $\sigma(e^+e^- \to Z^0 \to q^*q) \times BR(q^* \to q\gamma)$ (dotted curve) and of: $\sigma(e^+e^- \to H^0 + \text{hadrons}) \times BR(H^0 \to \gamma\gamma)$ (solid curve) as a function of M_{q^*} and M_{H^0}, respectively.

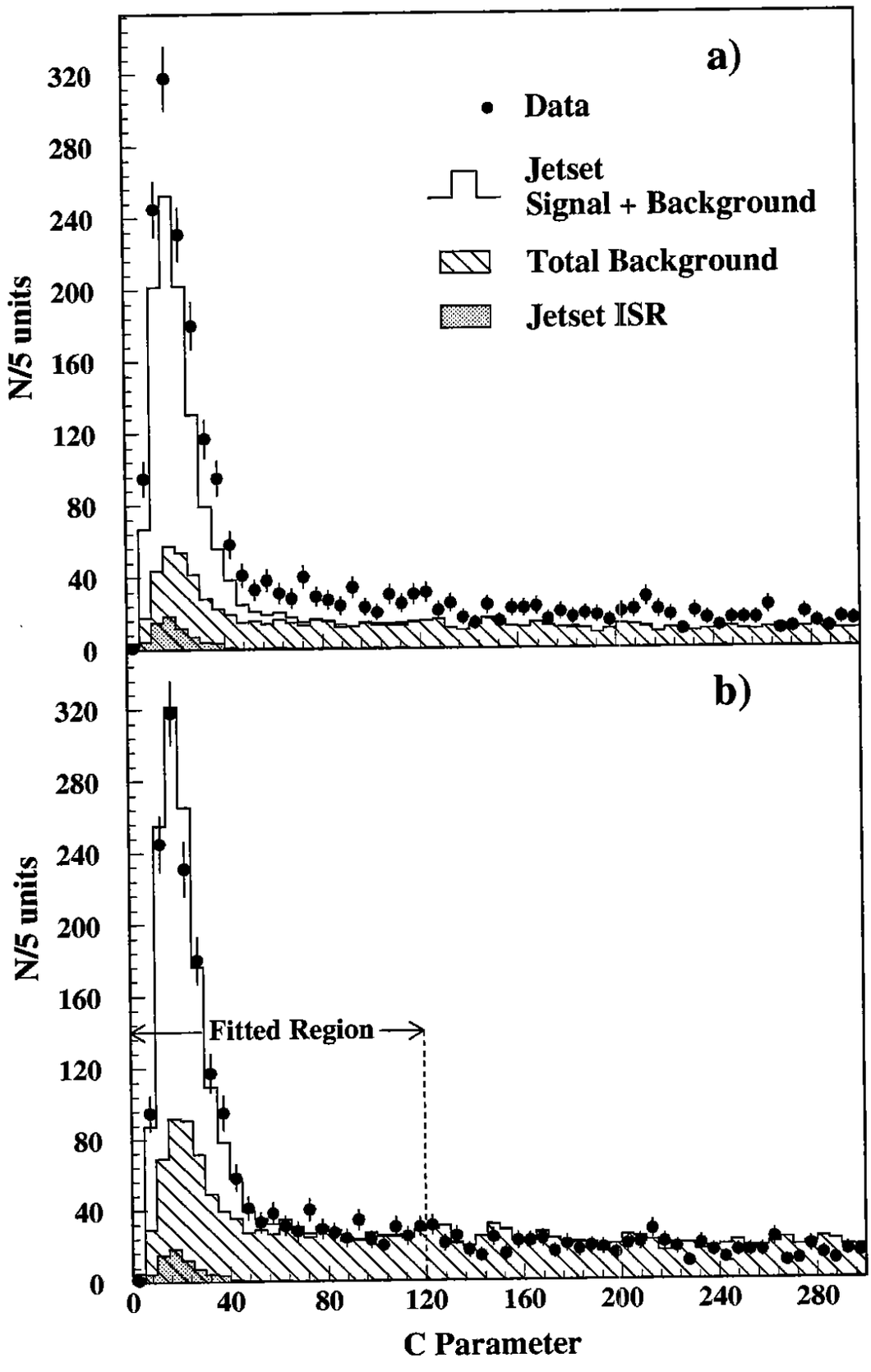
a)
Data
Jetset
Signal + Background
Total Background
Jetset ISR
N/5 units
320
280
240
200
160
120
80
40
0
b)
N/5 units
Fitted Region
0
40
80
120
160
200
240
280
C Parameter

Figure 1

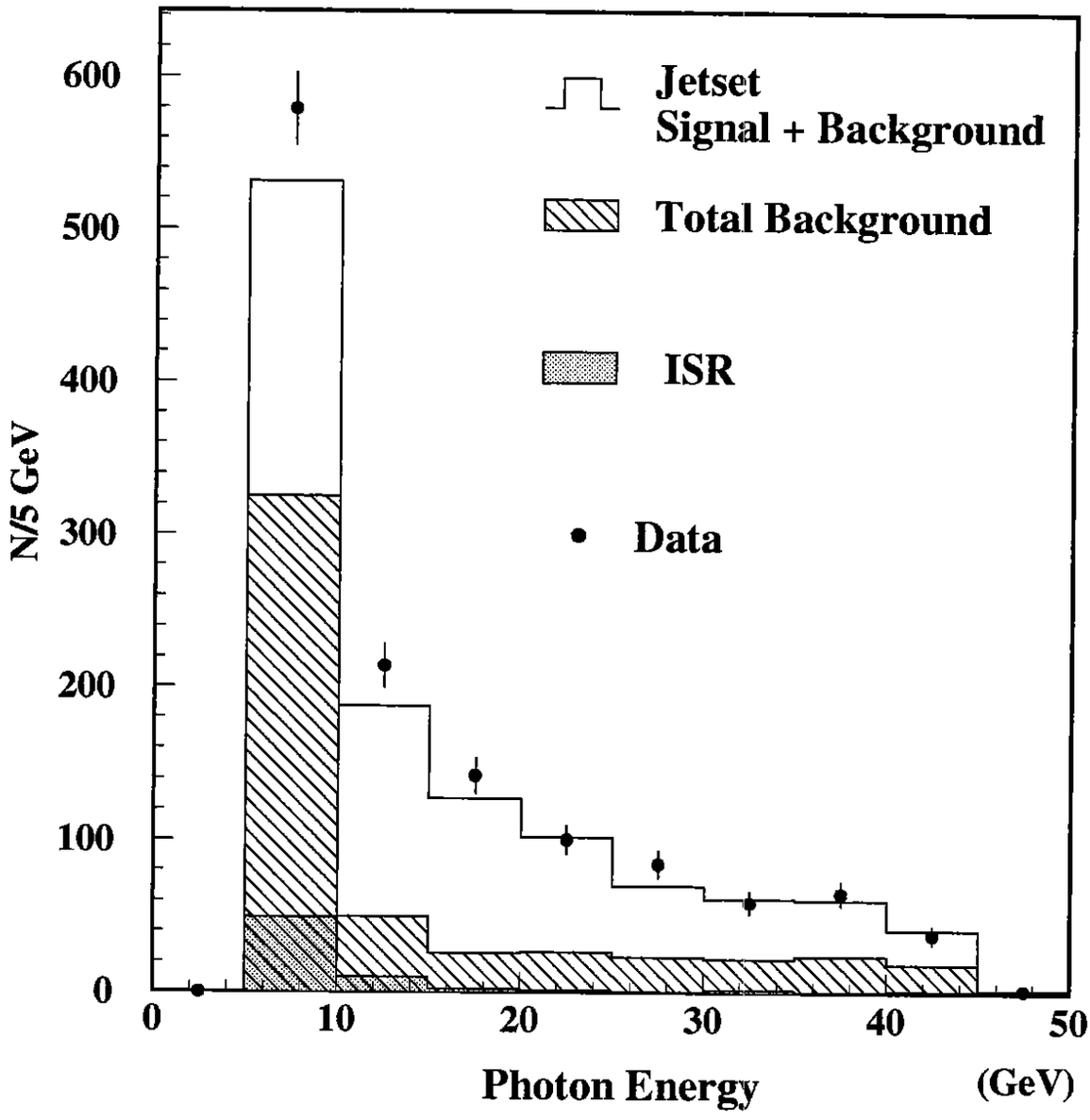
Jetset
Signal + Background
Total Background
ISR
Data
N/5 GeV
600
500
400
300
200
100
0
0
10
20
30
40
50
Photon Energy
(GeV)

Figure 2

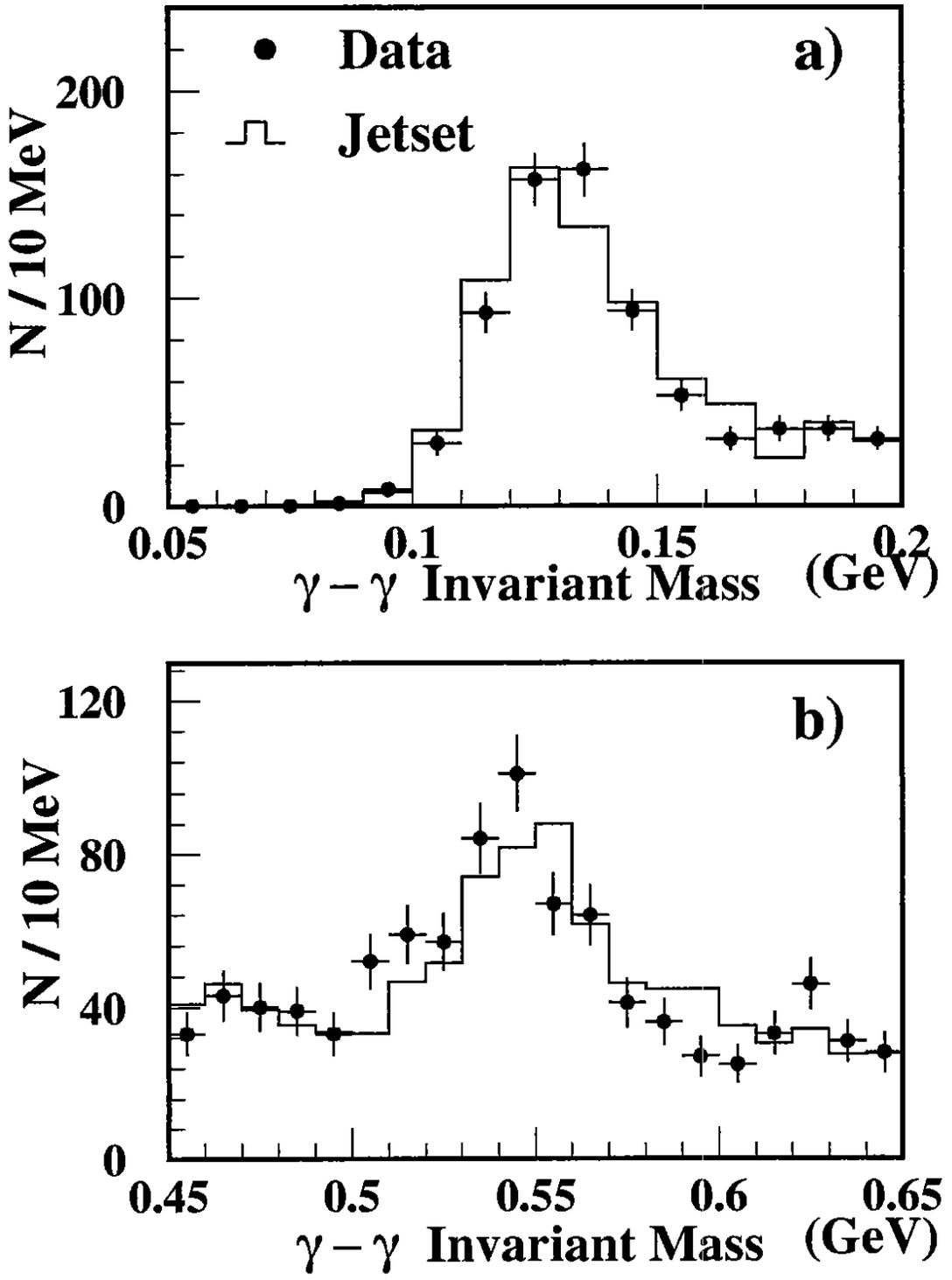
Data
Jetset
a)
N / 10 MeV
200
100
0
0.05
0.1
0.15
0.2
γ – γ Invariant Mass (GeV)
b)
N / 10 MeV
120
80
40
0
0.45
0.5
0.55
0.6
0.65
γ – γ Invariant Mass (GeV)

Figure 3

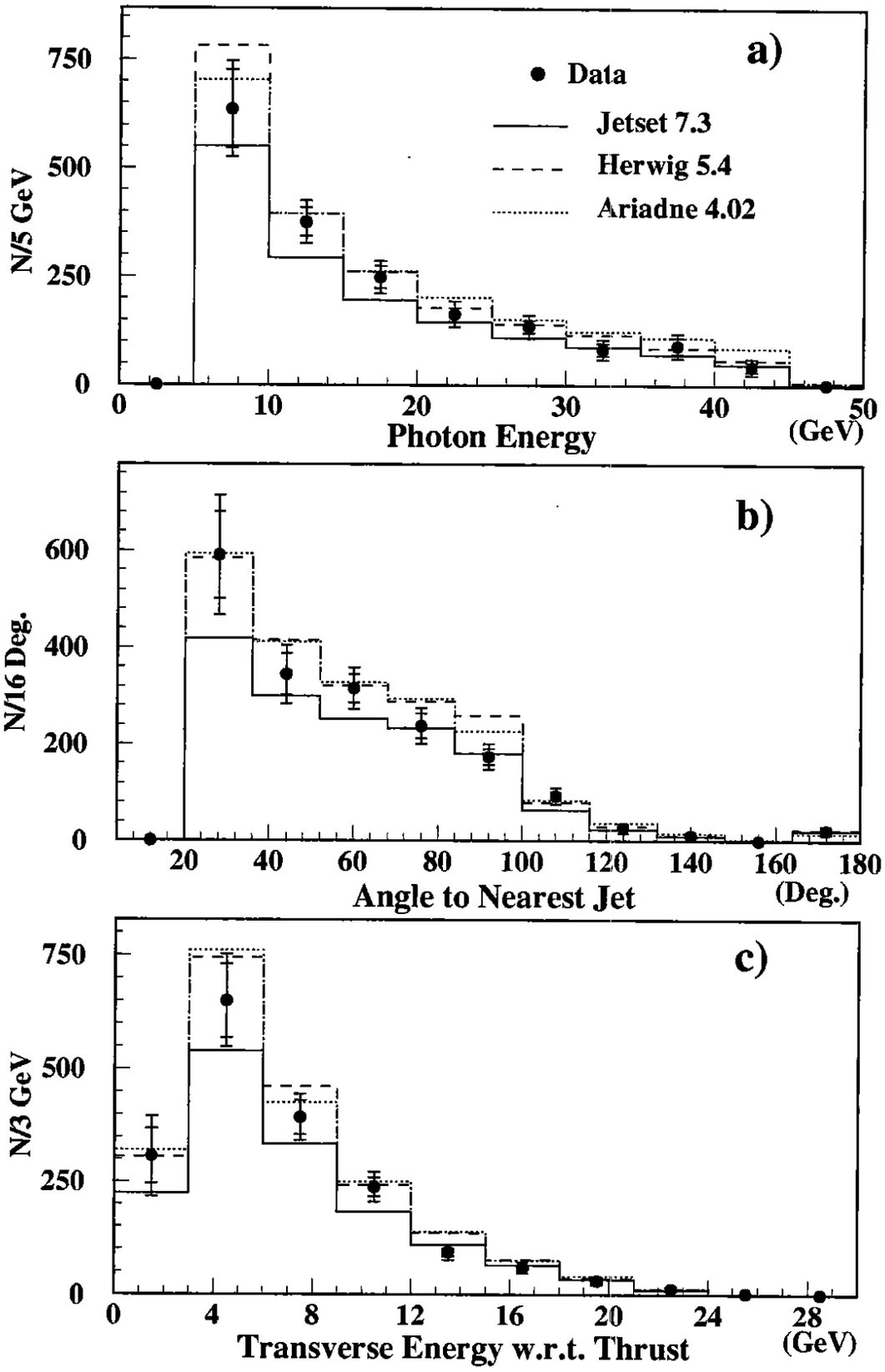
a)
Data
Jetset 7.3
Herwig 5.4
Ariadne 4.02
N/5 GeV
Photon Energy
(GeV)
b)
N/16 Deg.
Angle to Nearest Jet
(Deg.)
c)
N/3 GeV
Transverse Energy w.r.t. Thrust
(GeV)

Figure 4

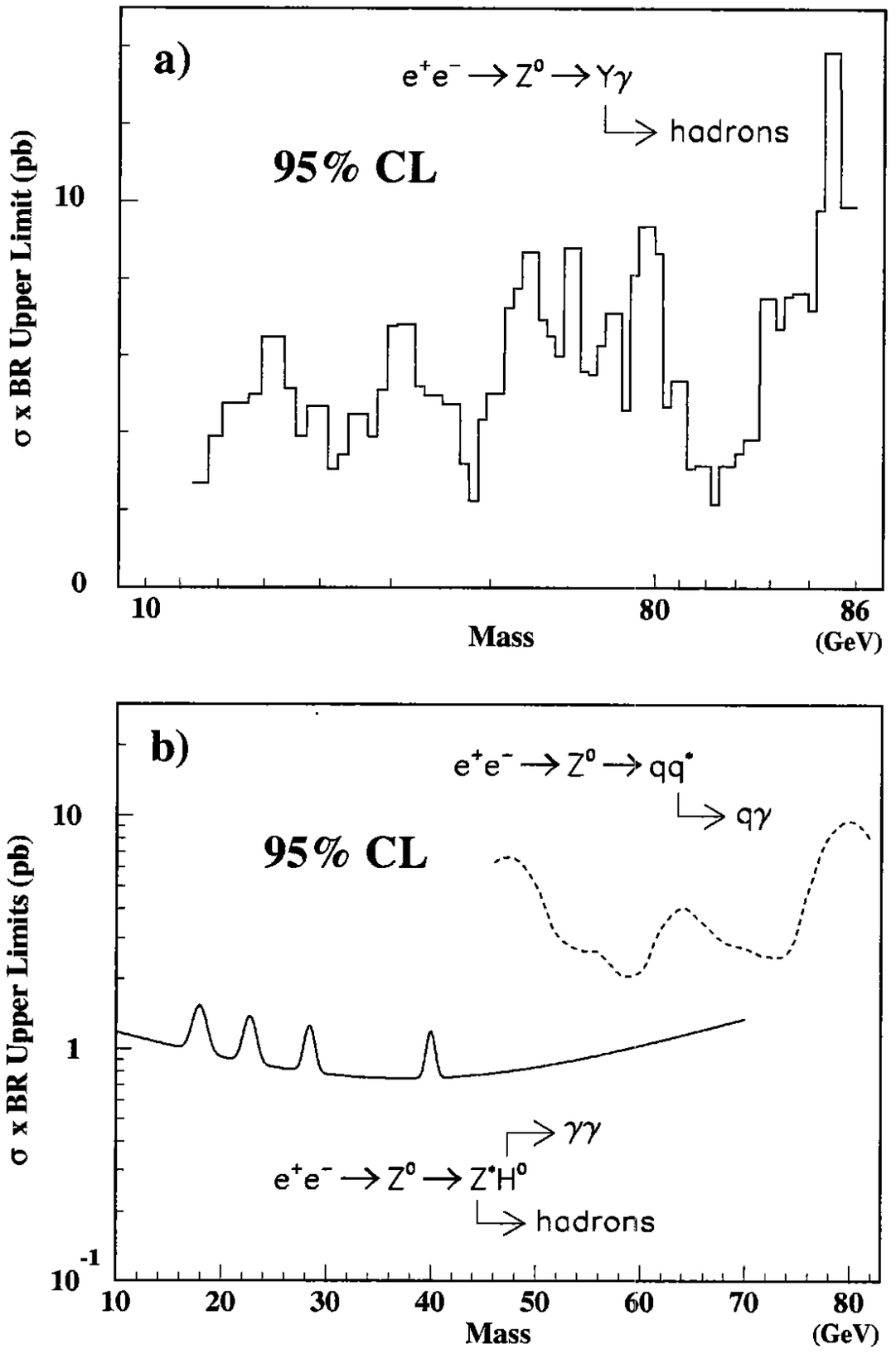
a)
$e^+e^- \to Z^0 \to Y\gamma$
hadrons
95% CL
σ x BR Upper Limit (pb)
10
0
10
80
86
Mass
(GeV)
b)
$e^+e^- \to Z^0 \to qq^*$
$q\gamma$
95% CL
σ x BR Upper Limits (pb)
10
1
10^{-1}
$\gamma\gamma$
$e^+e^- \to Z^0 \to Z^*H^0$
hadrons
10
20
30
40
50
60
70
80
Mass
(GeV)

Figure 5